

Connecting particle clustering and rheology in attractive particle networks: Supplementary information

Sebastian Bindgen, Frank Bossler[‡], Jens Allard, and Erin Koos*

KU Leuven, Chemical Engineering Department, Celestijnenlaan 200f, box 2424,
3001 Leuven, Belgium

* E-mail: erin.koos@kuleuven.be

[‡]Present address: Zeppelinstraße 1c, 85375 Neufahrn, Germany

List of Figures

S1	Example amplitude sweep data for two $\theta = 87 \pm 8^\circ$ samples.	2
S2	Confocal 2D images of phase separated samples	2
S3	Representative 3D structures for points I, II and III for $\theta = 87 \pm 8^\circ$	3
S4	Representative 3D structures for points IV, V and VI for $\theta = 87 \pm 8^\circ$. . .	4
S5	Representative 3D structures for points VII, VIII and IX for $\theta = 87 \pm 8^\circ$.	5
S6	Representative 3D structures for points I, II and III for $\theta = 115 \pm 8^\circ$. . .	6
S7	Representative 3D structures for points IV, V and VI for $\theta = 115 \pm 8^\circ$. .	7
S8	Representative 3D structures for points VII, VIII and IX for $\theta = 115 \pm 8^\circ$.	8
S9	Zoom of the structural parameters for $\theta = 87 \pm 8^\circ$ sample for low values of added, secondary fluid.	9
S10	Dependence of different values for the clustering coefficient on the amount of added, secondary fluid	9
S11	Direct relationship between the structural parameters and dynamic moduli.	10
S12	Histograms of betweenness centrality and corresponding averages for the $\theta = 87 \pm 8^\circ$ samples.	11
S13	Histograms of betweenness centrality and corresponding averages for the $\theta = 115 \pm 8^\circ$	12

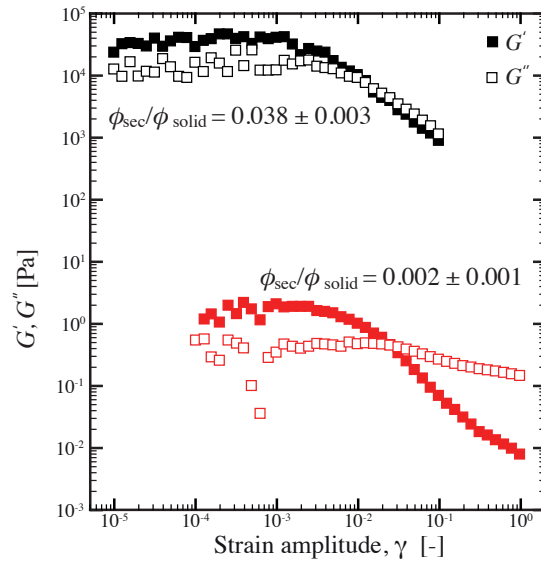


Figure S1: Example amplitude sweep data for two $\theta = 87 \pm 8^\circ$ samples.

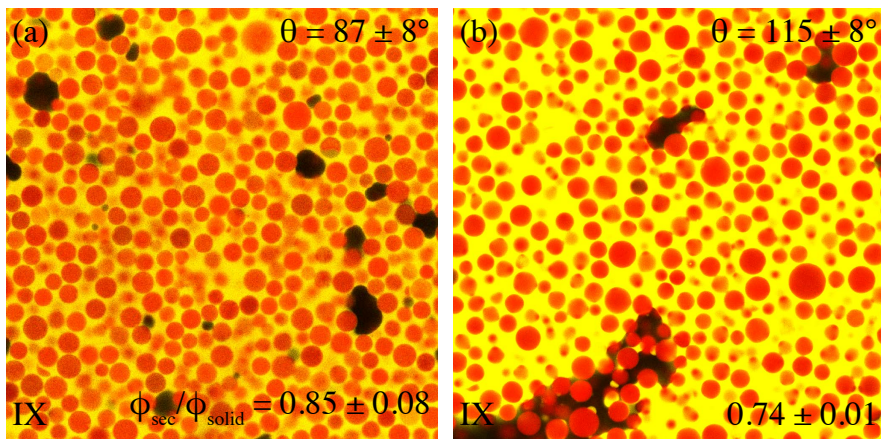


Figure S2: Confocal 2D images of phase separated samples (point IX) with (a) $\theta = 87 \pm 8^\circ$ and (b) $\theta = 115 \pm 8^\circ$.

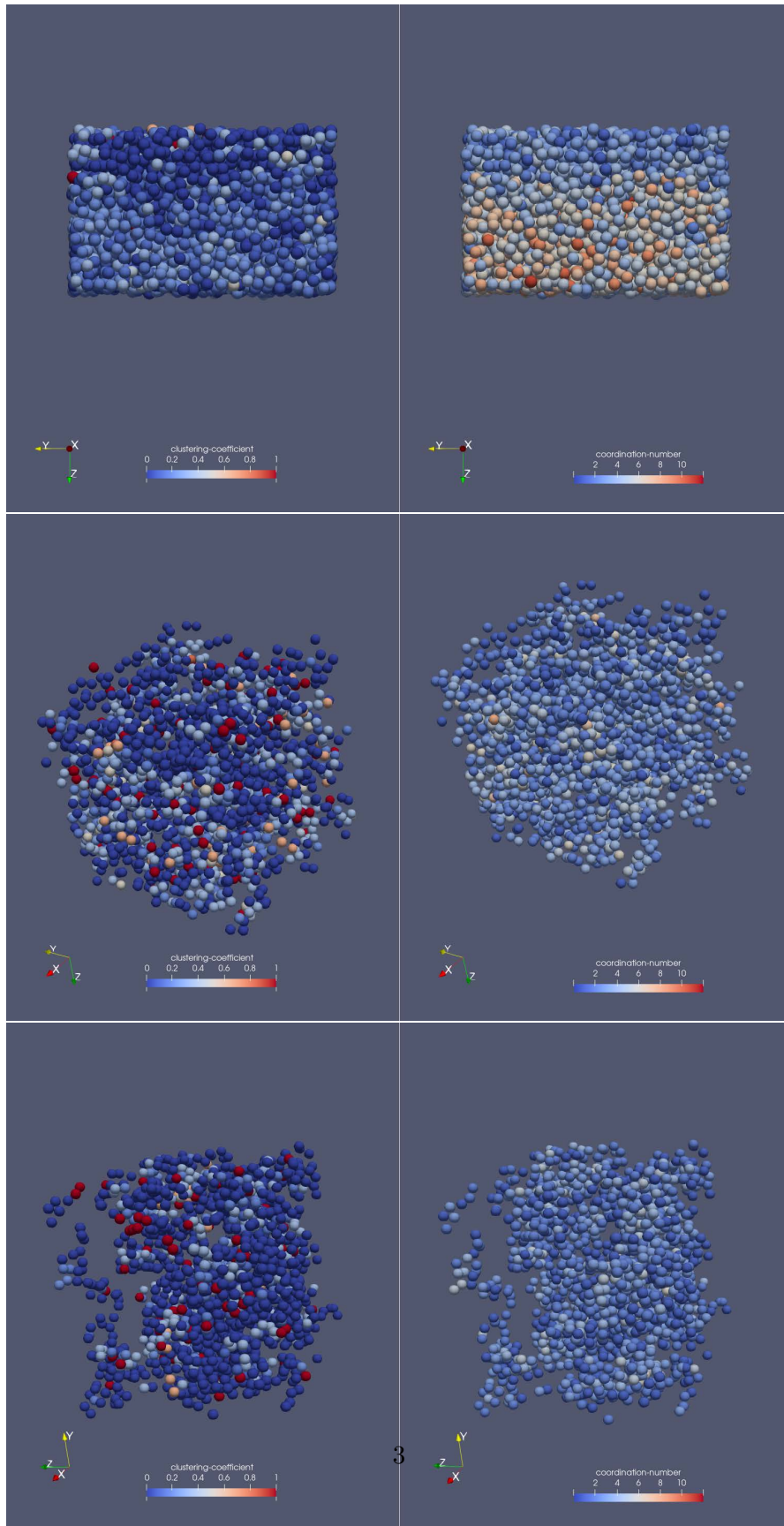


Figure S3: Representative 3D structures for points I, II and III with a contact angle of $\theta = 87 \pm 8^\circ$ for several amounts of secondary fluid.

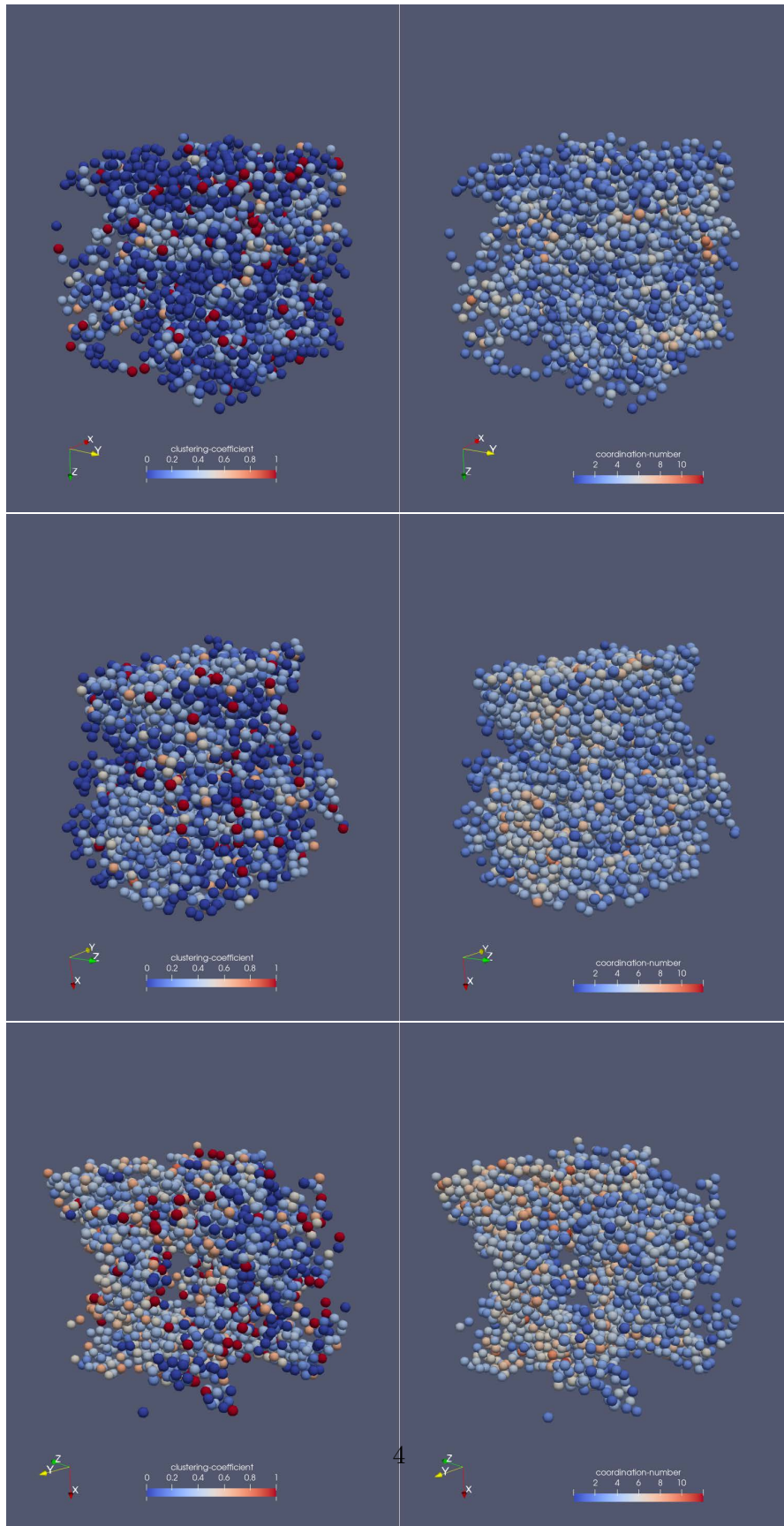


Figure S4: Representative 3D structures for points IV, V and VI with a contact angle of $\theta = 87 \pm 8^\circ$ for several amounts of secondary fluid.

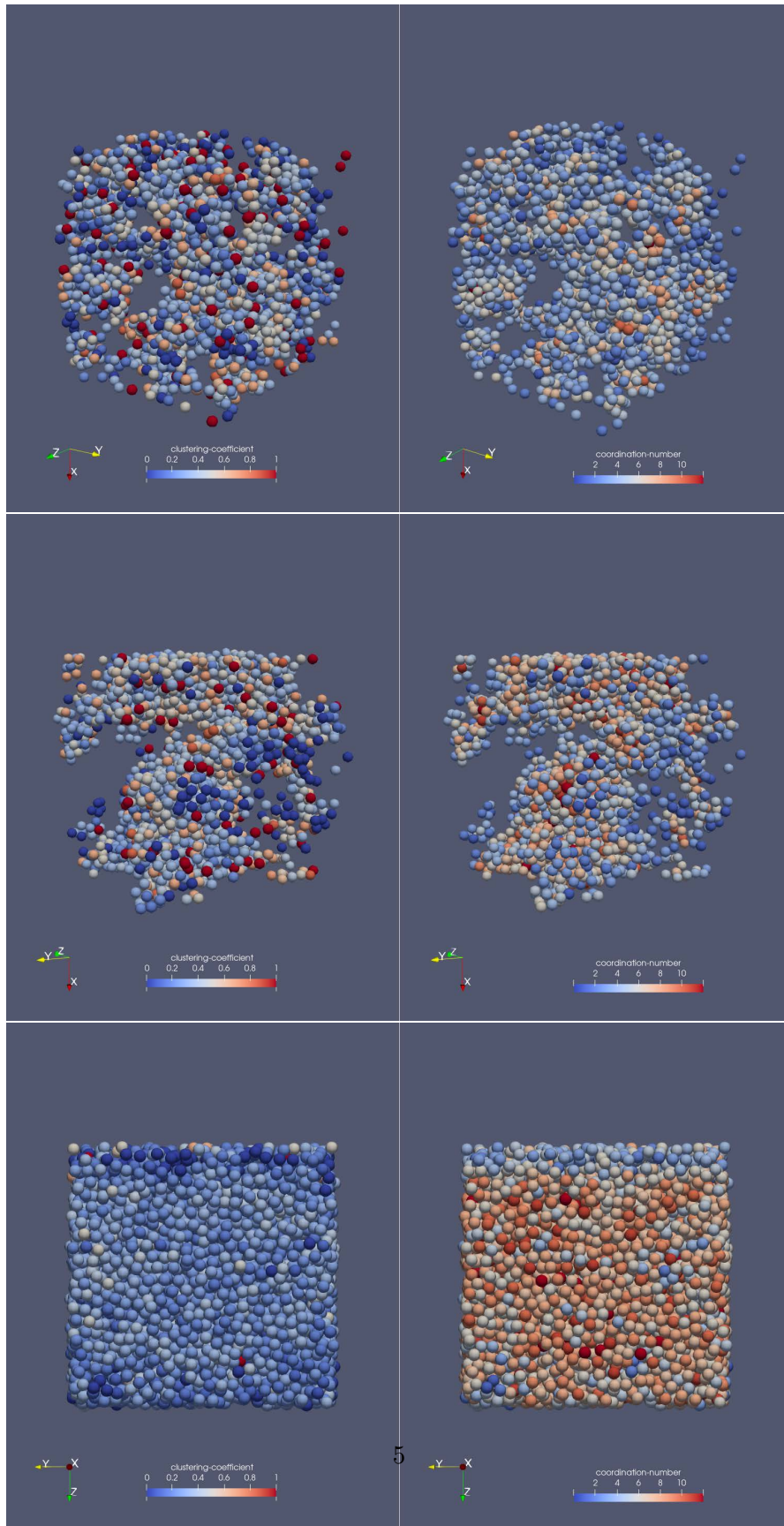


Figure S5: Representative 3D structures for points VII, VIII and IX with a contact angle of $\theta = 87 \pm 8^\circ$ for several amounts of secondary fluid.

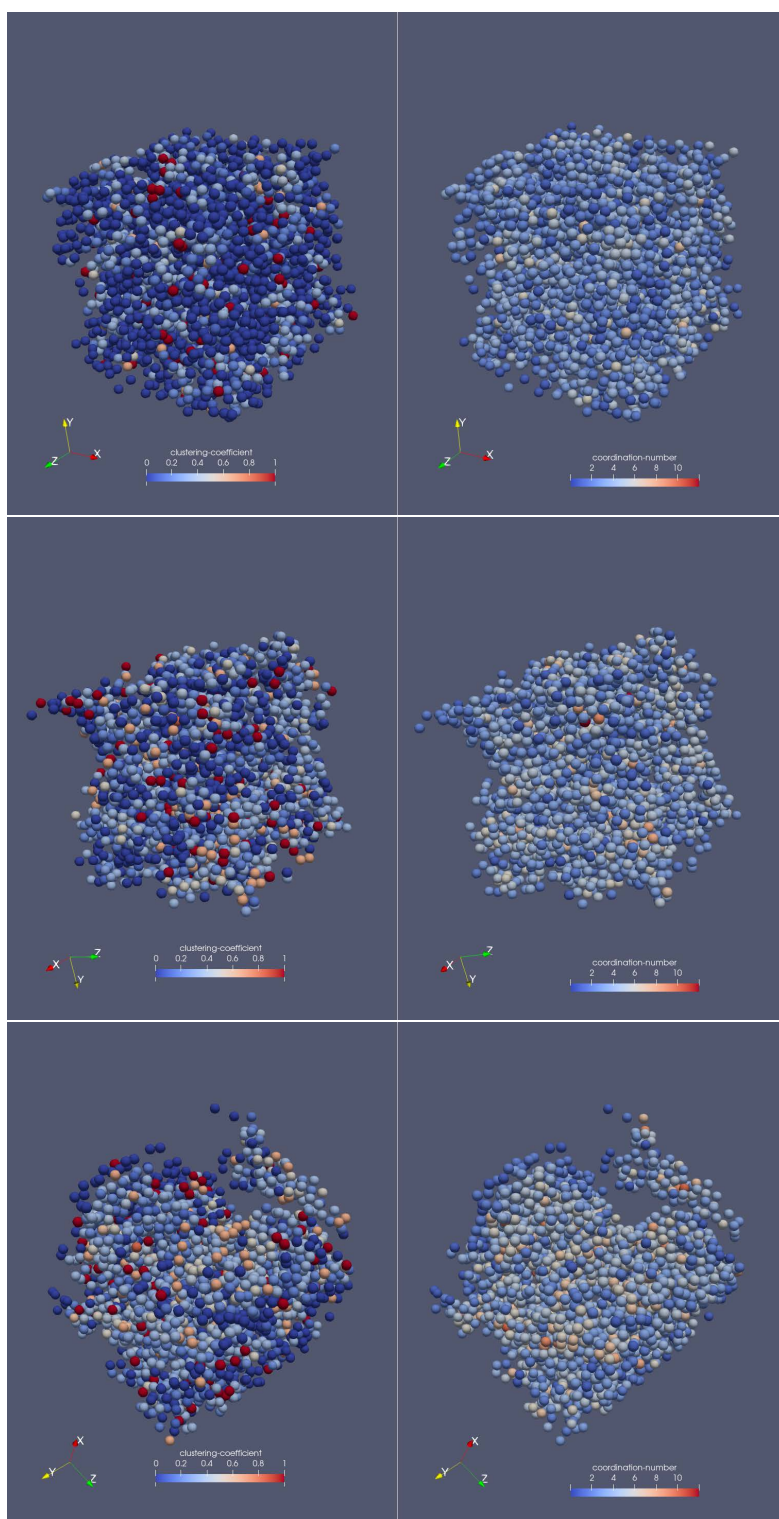


Figure S6: Representative 3D structures for points I, II and III with a contact angle of $\theta = 115 \pm 8^\circ$ for several amounts of secondary fluid.

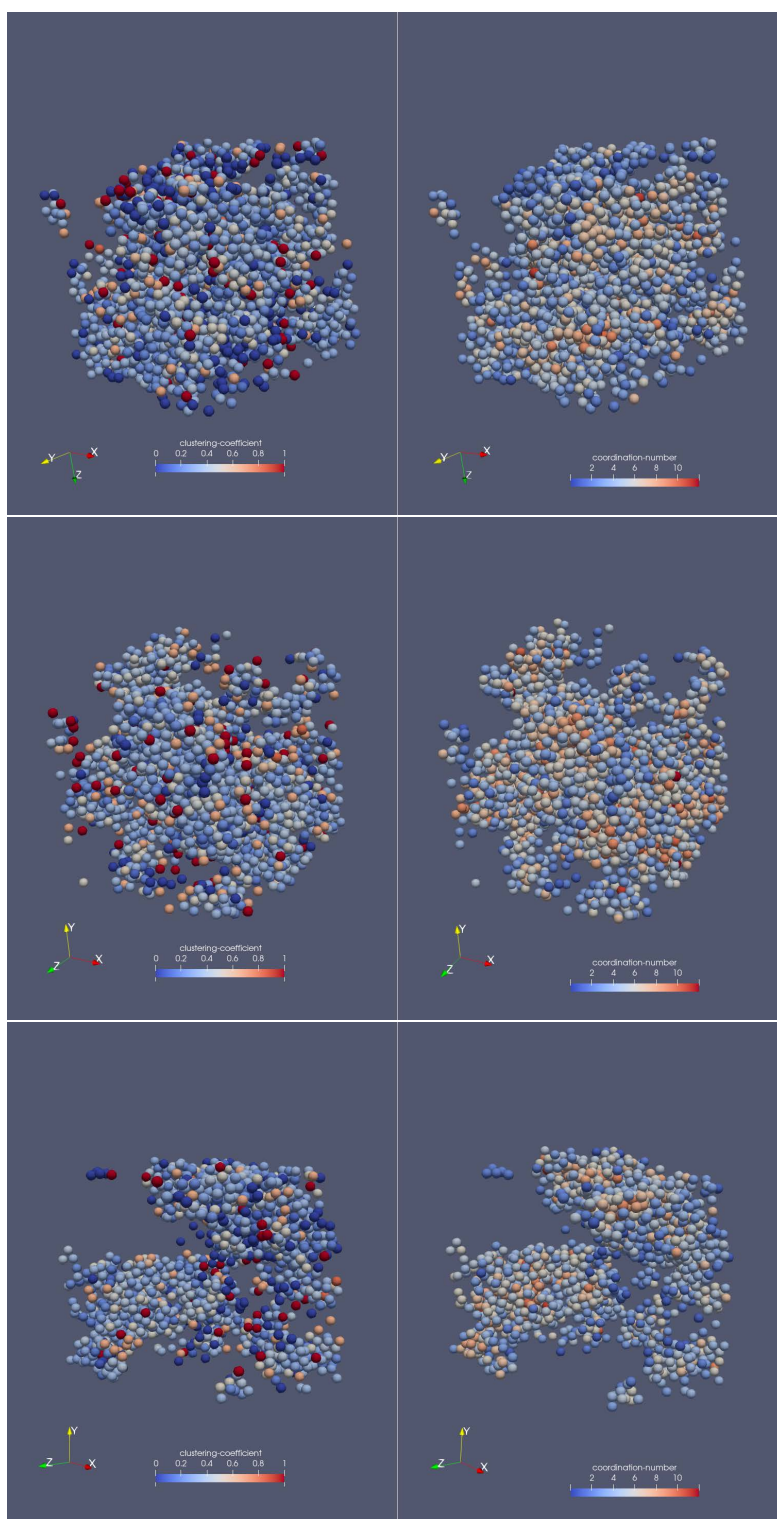


Figure S7: Representative 3D structures for points IV, V and VI with a contact angle of $\theta = 115 \pm 8^\circ$ for several amounts of secondary fluid.

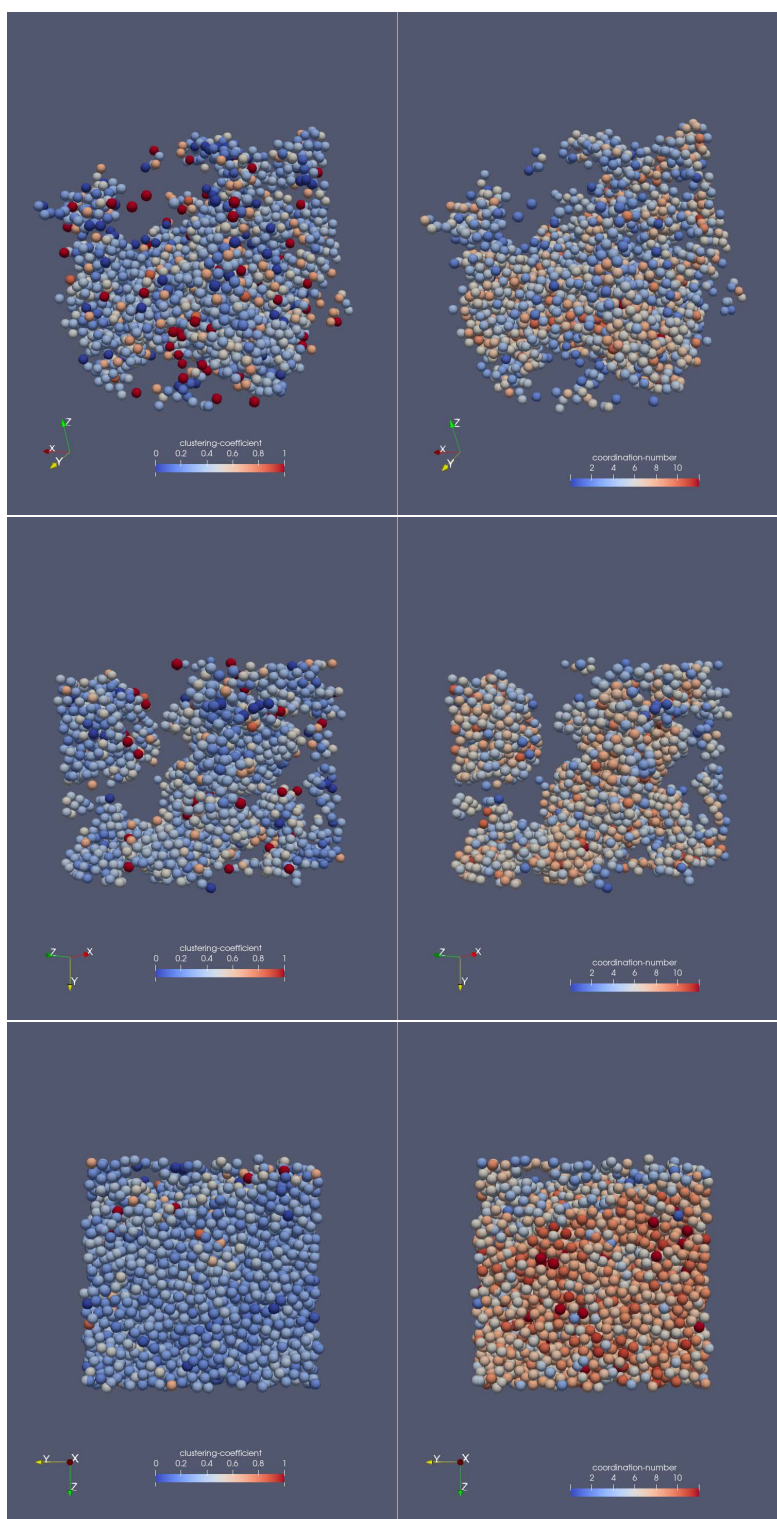


Figure S8: Representative 3D structures for points VII, VII and IX with a contact angle of $\theta = 115 \pm 8^\circ$ for several amounts of secondary fluid.

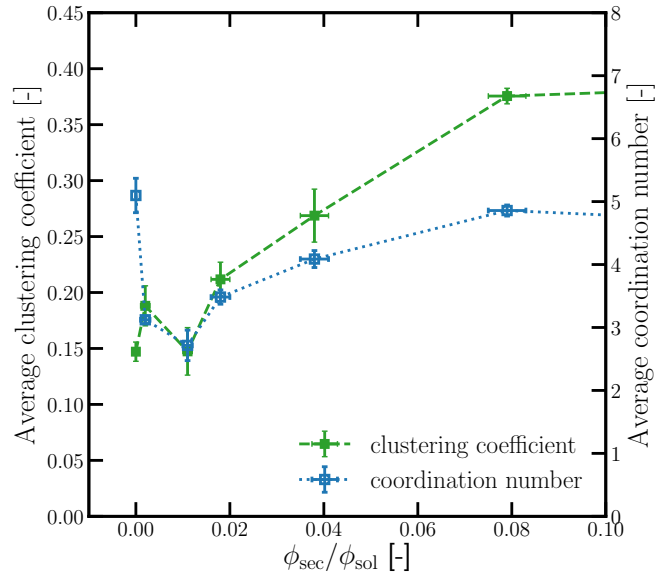


Figure S9: Zoom of the structural parameters for $\theta = 87 \pm 8^\circ$ sample for low values of added, secondary fluid.

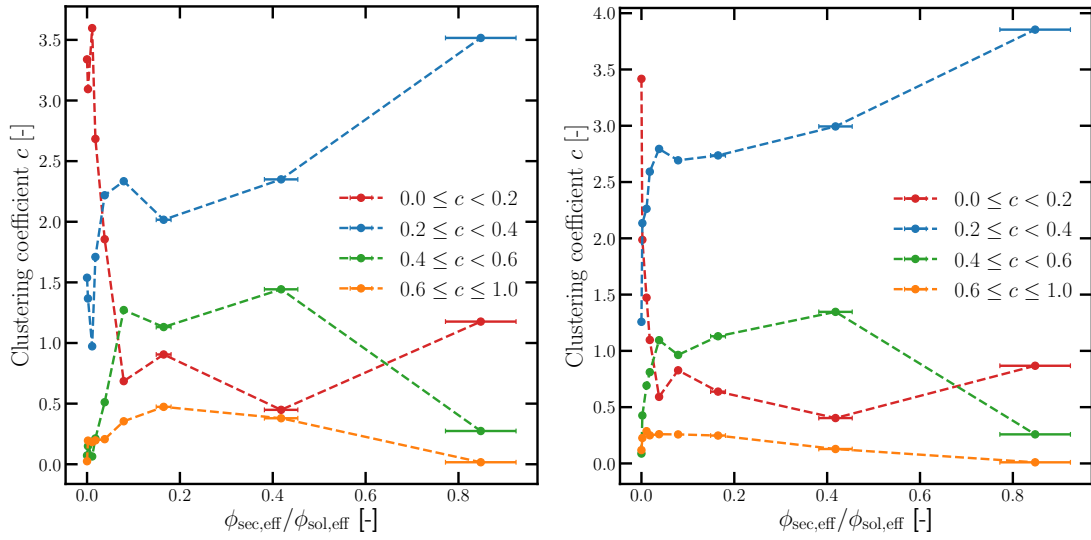


Figure S10: Dependence of different values for the clustering coefficient c on the amount of added, secondary fluid for the sample with (left) $\theta = 87 \pm 8^\circ$ and (right) $\theta = 115 \pm 8^\circ$.

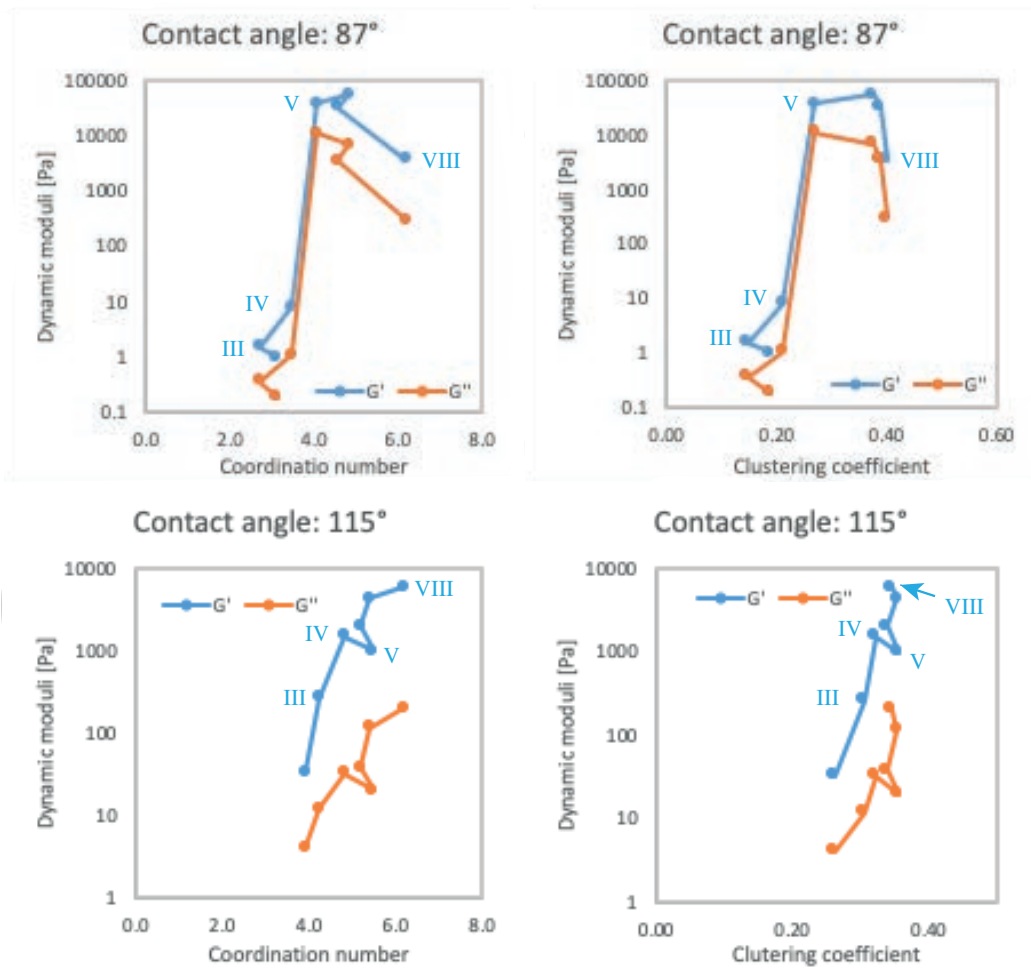


Figure S11: Direct relationship between the structural parameters and dynamic moduli.

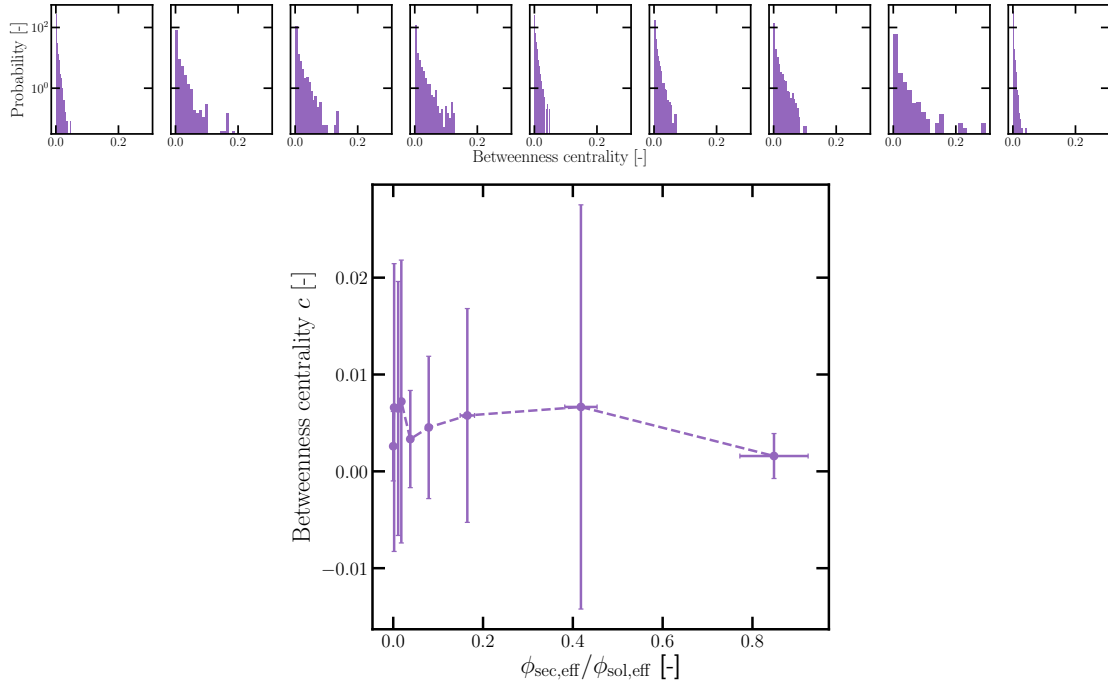


Figure S12: Histograms of betweenness centrality and corresponding averages for the $\theta = 87 \pm 8^\circ$ samples.

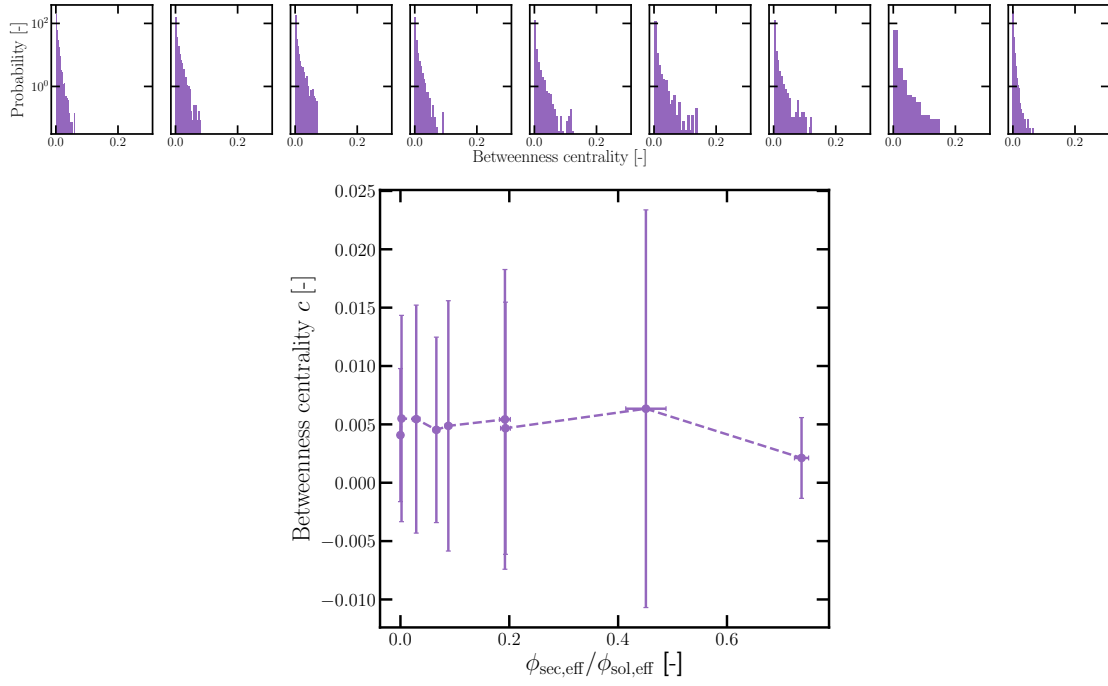


Figure S13: Histograms of betweenness centrality and corresponding averages for the $\theta = 115 \pm 8^\circ$.